Demonstration of protein capture and separation using 3D printed anion exchange monoliths fabricated in one-step

Demonstration of protein capture and separation using 3D printed anion exchange monoliths fabricated in one-step

Ursula Simon[1], Livia C T Scorza[2], Sarah Teworte[1], Alistair J McCormick[2] & Simone Dimartino[1]*

[1] Institute for Bioengineering, School of Engineering, The University of Edinburgh, Edinburgh EH9 3BF, UK.

[2] SynthSys & Institute of Molecular Plant Sciences, School of Biological Sciences, University of Edinburgh, Edinburgh, EH9 3BF, UK

* Corresponding author: Dr Simone Dimartino, Faraday Building, Colin McLaurin Road, The King's Buildings, Edinburgh EH9 3DW, UK, Phone: +44 131 6507305, Email: simone.dimartino@ed.ac.uk

Abstract

3D printing applications in separation science are currently limited by the lack of materials compatible with chromatographic operations and 3D printing technologies. In this work, we propose a new material for Digital Light Processing printing to fabricate functional ion exchange monoliths in a single step. Through copolymerisation of the bi-functional monomer 2-(Acryloyloxy)ethyl] trimethylammonium chloride, monolithic structures with quaternary amine ligands were fabricated. The novel formulation was optimised in terms of protein binding and recovery, microporous structure and its swelling susceptibility by increasing its crosslink density and employing cyclohexanol and dodecanol as pore forming agents. In static conditions, the material demonstrated a maximum binding capacity of 104.2 ± 10.6 mg/mL for BSA, in line with commercially available materials. Its anion exchange behaviour was validated by separating BSA and myoglobin on a

Received: 03/07/2020; Revised: 27/08/2020; Accepted: 28/08/2020

This article has been accepted for publication and undergone full peer review but has not been through the copyediting, typesetting, pagination and proofreading process, which may lead to differences between this version and the Version of Record. Please cite this article as doi: 10.1002/jssc.202000722.

monolithic bed with Schoen gyroid morphology. The same column geometry was challenged for the purification of C-phycocyanin from clarified as well as cell-laden *Arthrospira platensis* feedstocks. This represents the first demonstration of one-step printed stationary phases to capture proteins directly from solid-laden feedstocks. We believe that the material here presented represents a significant improvement towards implementation of 3D printed chromatography media in the field of separation science.

Keywords: 3D printing materials, Anion exchange monolith, Protein adsorption, Digital Light Processing, C-phycocyanin

Abbreviations

AETAC – 2-(Acryloyloxy)ethyl] trimethylammonium chloride

A. platensis – *Arthrospira platensis*

CPC – C-phycocyanin

DEGEEA – Di(ethylene glycol) ethyl ether acrylate

Digital Light Processing – DLP

EBA – Expanded bed adsorption

MYO – Myoglobin

PEGDA - Polyethylene glycol diacrylate

QA – Quaternary Amine

1. Introduction

Chromatographic separations currently rely on randomly packed spherical adsorber beads, with slurry packing procedures being the only economical and feasible method for column packing. However, computer simulation have demonstrated that ordered structures have the potential to greatly improve separation performances [1,2]. With the introduction of 3D printers, it is now

feasible to fabricate stationary phases with ordered three-dimensional morphology according to digital models [3].

The suitability of 3D printing to create ordered structures for chromatographic applications has been previously demonstrated. In 2014, Nawada et al. [4] experimentally proved that ordered beds were endowed with lower height equivalent to a theoretical plate (HETP) than randomly packed beds, as earlier suggested by simulations [1,2]. However, the commercial materials employed did not allow for the testing of protein separation due to their lack of suitable chromatographic ligands. McDonald et al. [5] employed a commercial material (Veroclear-RGD810, Stratasys Ltd.) for 3D printing that displayed a net negative surface charge to enable separation of a range of test components, such as dyes and proteins. However, commercial materials for 3D printing are non-porous and with proprietary composition, limiting their application in chromatography. According to a different preparation method, commercial materials for 3D printing can be used to fabricate sacrificial moulds, which are then infused with a traditional material for chromatography such as porous agarose or cellulose hydrogels, followed by chemical modification for the introduction of the chromatographic ligand [6].

In 2019 we proposed new material formulations compatible with commercial 3D printers but also bearing appropriate chromatographic functionality [7]. There, we demonstrated full integration of 3D printing technology to manufacture monolithic stationary phases in one simple step. The one-step fabrication method proposed was based on the bifunctional monomer 2-(Acryloyloxy)ethyl] trimethylammonium chloride (AETAC), bearing a positively charged quaternary amine (QA) group as well as a 3D printable acrylate group in its structure (

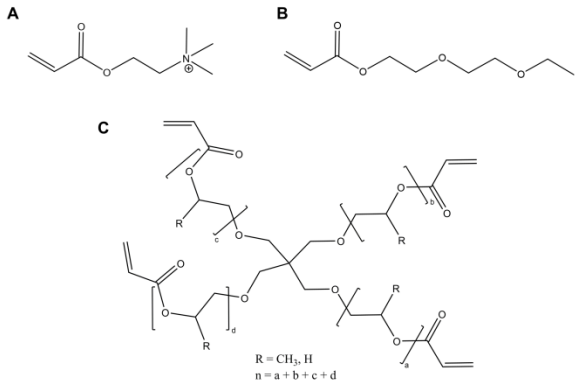

Figure 1).

In this work, we present our recent material optimization efforts with crucial key improvements with respect to the first version of the QA material presented in 2019. After determining the best ligand density for BSA adsorption in static adsorption experiments, we demonstrate, for the first time, the separation of BSA and myoglobin (MYO) in dynamic conditions using a QA functional monolith with Schoen gyroid bed geometry. Subsequently, we investigated the potential of the 3D printed monolith to purify C-phycocyanin (CPC), a blue phycobiliprotein produced in cyanobacteria and algae [8]. CPC is a high value product widely used in the food, cosmetic and pharmaceutical industries as a naturally derived blue pigment [9]. In this study we used the monolith to purify CPC directly from crude CPC extracts of the cyanobacterium *Arthrospira platensis (A. platensis)* in a single step chromatographic method.

2. Materials and Methods

A detailed description for the protein adsorption in batch conditions, protein purification in dynamic conditions, purification of C-phycocyanin, sample preparation for scanning electron microscopy, and a flowchart of the custom-built chromatography system are available in the Supporting Information.

2.1. Materials

2-(Acryloyloxy)ethyl] trimethylammonium chloride (AETAC, 80 wt % in water), di(ethylene glycol) ethyl ether acrylate (DEGEEA, technical grade ≥ 90 %), ethanol (absolute, HPLC grade, ≥ 99.8 %), hexamethyldisilazane (≥ 99.9 %), myoglobin (MYO, equine heart), Trizma® base and hydrochloride were obtained from MilliporeSigma (St. Louis, MO, USA). 1-dodecanol, bovine serum albumin (BSA, protease free powder), cyclohexanol , sodium chloride, sodium phosphate mono and dibasic were purchased from Fisher Scientific (Hampton NH, USA). Polyethylene glycol diacrylate (PEGDA, SR259, average MW 200 g/mol) and alkoxylated pentaerythritol tetraacrylate (SR494) were kindly donated by Arkema-Sartomer (Colombes, France). Phenyl bis(2,4,6-trimethylbenzoyl)-phosphine oxide

(Omnirad 819) and Tinuvin 326 were kindly provided by IGM resins (Waalwijk, The Netherlands) and BASF (Ludwigshafen, Germany), respectively. All chemicals were used as received.

2.2. 3D printing material preparation

The 3D printing material was prepared by dissolving 1 g of the photoinitiator Omnirad 819 and 0.125 g of the photoabsorber Tinuvin 326 in 100 mL of the pre-printing mixture composed of 48 % (v/v) cyclohexanol, 12 % (v/v) 1-dodecanol, 12 % (v/v) PEGDA, 12 % (v/v) SR494 and 16 % (v/v) monomer mixture (AETAC & DEGEEA). Materials with QA ligand densities of 2.33, 1.73, 1.14 and 0.57 mmol/mL were obtained by using monomer mixture having 100, 75, 50, 25 % (v/v) AETAC in DEGEEA , respectively, with 0 % AETAC employed as control material. The prepared printing material was stored covered in aluminium foil to prevent uncontrolled polymerisation until usage.

2.3. 3D Model creation and 3D printing

For static protein batch adsorption, hollow cylinders fitting into 96-microplate wells (Figure 2-A, B) were designed as described in [7]. For dynamic separation experiments, a monolithic column with Schoen gyroid geometry was employed. This structure was obtained from a Schoen gyroid unit cell (2π x 2π x 2π) generated in Wolfram Mathematica 12 (Wolfram Research Inc., Champaign, IL, USA) according to equation (1):

$$\sin(x) \cdot \cos(y) + \sin(y) \cdot \cos(z) + \sin(z) \cdot \cos(x) = 0 \quad (1)$$

The unit cell was then scaled to a side length of 1 mm (corresponding to wall thickness of 500 µm), replicated in the three dimensions, and assembled into a cylindrical column (5 mm radius, 20 mm length) using Netfabb 2017 (Autodesk, San Rafael, CA, USA).

Both models were sliced into 100 µm thick 2D layers using Netfabb 2017 and 3D printed using a Solflex 350 digital light processing (DLP) printer (W2P Engineering GmbH, Vienna, Austria). After

printing, all 3D printed parts were extensively cleaned in ethanol on a roller mixer (SRT9D, Stuart, Staffordshire, UK). Parts were stored in 20 % (v/v) ethanol until further use.

3. Results and Discussion

In this work, a DLP printer was employed for the direct 3D printing of QA-functionalized chromatographic adsorber. DLP 3D printing materials are complex mixtures composed of photopolymerisable monomers and crosslinkers forming the polymeric network, photoinitiators required to start the photopolymerisation reaction and photoabsorber to increase the printing resolution [10,11]. These formulations need to be adapted for use in chromatography by introducing suitable chromatographic ligands and porosities to increase binding capacity.

Strong anion exchange functionalities were embedded into the stationary phase due to incorporation of the bifunctional monomer AETAC in the parent formulation, providing positively charged quaternary amine (QA) groups (

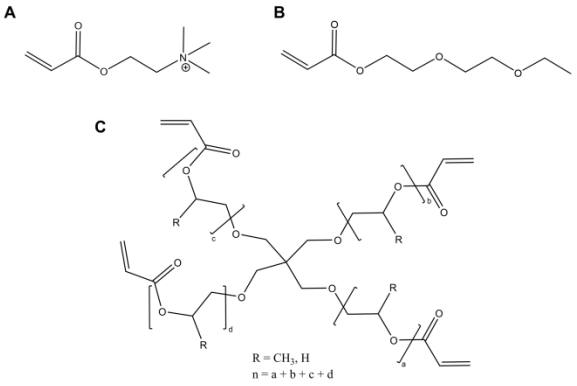

Figure 1-A) [12]. Material porosity was achieved by introducing porogenic solvents soluble in the printing formulation but not taking part to the polymerisation reaction [13].

3.1. Optimization of material formulation

The scope of this work was to optimise the previously published QA 3D printing material [7] in terms of protein adsorption, protein recovery as well as its compatibility with current chromatography processes. By changing the material composition, the following main challenges have been addressed:

1. *Optimization of bind and elute characteristics*. In previous batch adsorption experiments [7], higher protein binding capacities were achieved by decreasing the ligand densities. Also, recovery over the elution step was of only about 10 % or less (Figure 3-B), a result associated with the stationary phase overcrowded with QA ligands leading to configuration change and irreversible adsorption. To further investigate these two observations, materials with lower concentrations of the QA-bearing monomer AETAC were prepared, leading to stationary phases with lower ligand densities. Di(ethylene glycol) ethyl ether acrylate (DEGEEA,

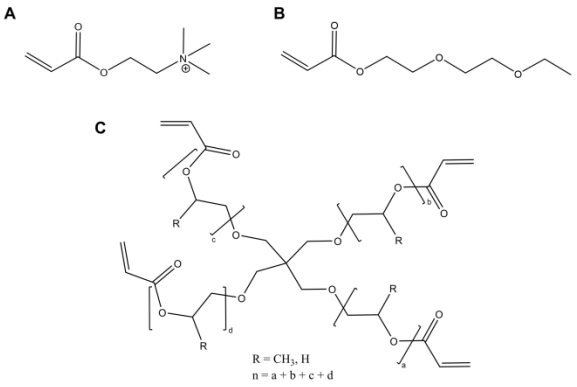

2. Figure 1-B) was introduced into the formulation as non-functional monomer to maintain a constant monomer to crosslinker ratio (40:60 volume based) while allowing changes in the QA ligand density. DEGEEA was chosen as non-functionalised monomer since it presents similar backbone to the PEGDA crosslinker employed and similar molar mass to the functional AETAC monomer. The influence of ligand density on binding and elution is further discussed in section 3.2.
3. *Optimization of the porous microstructure.* The PEG previously used as porogenic compound produced pores of relatively small size (10 – 20 nm) [14]. Small sized pores cause serious mass transfer limitations by hindering free diffusion along the porous network, effectively lowering the diffusion coefficient within the stationary phase. Pores of small size may also negatively impact on protein recovery over elution as irreversibly immobilized species further reduce the pore dimensions. A mixture of cyclohexanol and dodecanol was thus employed as porogens as

they are widely employed in traditional fabrication of monoliths [13,15,16]. SEM analysis (Figure 2-C) of monoliths produced with the new formulations shows a highly interconnected porous network, with pores in the 100 – 300 nm range as measured from the SEM images. Commercial chromatographic adsorber beads display pores in the order of 10 - 100 nm [17], hence, similar mass transfer rates are expected for the proposed material formulation.

4. *Optimization of mechanical properties*. Relatively low mechanical stability and significant swelling/shrinking upon buffer change were observed in [7]. This was corrected by increasing the density of crosslink bonds through the introduction of SR494 (

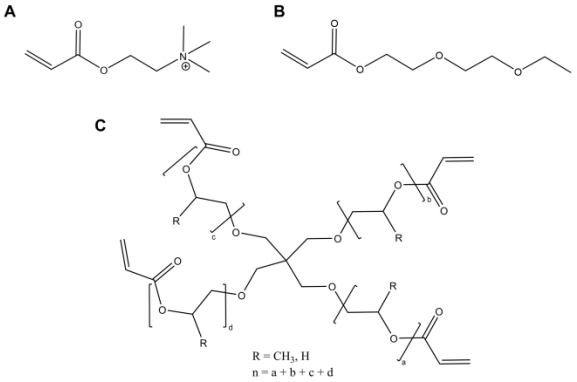

5. Figure 1-C), a supercrosslinker, providing four photopolymerisable acrylate groups per molecule and based on polyethylene glycol (PEG) motifs for low non-specific protein binding. As a compromise in providing chemical and mechanical strength as well as allowing the creation of a porous network, the supercrosslinker was employed in combination with PEGDA, the previously applied crosslinker providing two polymerisable acrylate groups. This provided mechanically stronger parts and limited shrinkage/swelling of the 3D printed structures upon buffer change. For instance, when the salt concentration was increased from 0 to 1 M NaCl, monoliths containing solely PEGDA as crosslinker demonstrated a pore volume shrinkage of 20 %, whereas using SR494 as crosslinker resulted in a decrease of only 12.5 % (Figure S2).
6. *Optimization of visual appearance*. Structures printed with the initial material formulation displayed red colour [7], indicating that some of the photoabsorber, the red dye reactive orange,

remained in the material despite extensive washing procedures. Reactive orange has a negative charge in its structure and binds tightly to the positive QA ligands by electrostatic interactions. The low concentration of reactive orange in the material formulation ensured availability of QA ligands for protein binding, but the red colouration was considered a nuisance for future commercial exploitation. Reactive orange was replaced by Tinuvin 326, a charge neutral light-yellow dye. This facilitated removal of the photoabsorber after printing to produce white structures (Figure 2).

3.2. Protein adsorption in batch experiments

The equilibrium binding capacity of materials with different ligand density (control, 0.57, 1.14, 1.73, 2.33 mmol/mL) was investigated, with resulting adsorption isotherms displayed in Figure 3-A. Adsorbers with hollow cylindrical shape fitting into wells of a 96-well microplate were printed to facilitate the adsorption experiment (Figure 2-A, B) [7]. This allowed in-situ measurement of protein concentration in the liquid phase using a plate reader. The equilibrium data measured were fitted using the Langmuir isotherm ($R^2 > 0.96$, best-fit parameters in Table 1). The highest maximum binding capacity of 104.2 ± 10.6 mg/mL was found for the material with a ligand density of 1.73 mmol/mL. Further increasing or decreasing the ligand density resulted in lower binding capacities (Figure 3-B), revealing a compromise between amount of exposed ligands and steric hindrance due to previously adsorbed biomolecules, which was in line with that of commercial chromatography materials [18,19]. The 3D printed materials previously tested [7] had larger ligand densities (2.03 - 3.18 mmol/mL) but lower binding capacities (up to 73.7 mg/mL) compared to the new materials presented in this work (Figure 3-B). It is worth noting that the trend of binding capacity with ligand density overlaps across the two material formulations (Figure 3-B), indicating that binding is principally, if not solely, due to the positive charges of the AETAC monomer. This is further confirmed by the results obtained with the control material containing no QA ligands which showed negligible protein adsorption. No protein adsorption for the control also validated the use of

this material formulation as stationary phase with low non-specific binding characteristics [20]. Protein recovery in the elution step showed a similar trend, with recovery peaking at 47.09 ± 5.06 % for the material with 1.73 mmol/mL ligand density. This suggested that BSA tends to bind strongly to the materials developed, potentially through a combination of ion and hydrophobic interactions. Yet, the newly developed materials had 5 x higher elution recoveries than the previous materials [7] (elution < 10 %, Figure 3-B), indicating a substantial improvement. To support future optimization of elution conditions, the mechanism behind the observed protein binding is currently investigated.

3.3. Protein separation and purification in dynamic mode

The best performing material (1.73 mmol/mL ligand density) was tested in dynamic conditions for the separation of a model protein mixture of BSA and MYO as well as the purification of CPC from a complex feedstock. The design freedom of 3D printing was further exploited by creating monoliths with Schoen gyroid bed geometry (Figure 2-D,E,F). Schoen gyroids are part of the triply periodic minimal surface family which are impossible to create with traditional manufacturing methods. Advantages of the Schoen gyroid geometry include excellent structural strength, high permeability and interconnected pathways [21,22]. In computer simulations, they have demonstrated HETP values than ordered spherical beads thanks to their uniform flow channels [23]. A Schoen gyroid structure was chosen as stationary phase geometry due to its superior HETP characteristics compared to randomly packed beds [23]. A monolith with 500 µm walls and 50 % porosity was designed and 3D printed (Figure 2-D, E). The cylindrical monolith was then introduced into a glass column (Figure 2-F) and connected to a chromatography system.

3.3.1.Separation of BSA and myoglobin from clarified solutions

A 1.6 mL column was employed for the separation of a model protein mixture of BSA and MYO. Three runs were carried out to demonstrate protein separation and reproducibility over subsequent runs. The chromatograms obtained, presented in Figure 4, show a first initial peak corresponding to the flow through, followed by two peaks over the salt gradient applied (0 – 300 mM NaCl over

20 CV). The first peak (retention volume of 7.4 ± 0.1 CV, ionic strength of 3.1 mS/cm) corresponds to elution of MYO as confirmed by control experiments obtained by an injection of pure MYO (7.7 + 0.01 CV, 3.6 mS/cm). The second peak (18.7 ± 0.1 CV, 19.0 mS/cm) corresponds to elution of BSA, as substantiated in a control run with pure BSA (retention volume 18.0 ± 0.7 mL, 18.4 mS/cm). The observed elution order is in line with the pI of the two proteins (pI_{MYO} = 7.0, pI_{BSA} = 4.8), demonstrating separation behaviour in line with ion exchange interactions. The three consecutive separation runs showed great reproducibility in terms of protein retention time (relative error 0.4 to 2.3 %) as well as observed peak areas (relative error 3.7 to 8 %), showcasing the robustness of the novel material and fabrication method presented.

A wall thickness of 500 µm was chosen to ensure prints of consistently good quality, at the expense of incomplete protein adsorption and band broadening effects. This is basically due to protein diffusion through the relatively thick stationary phase as the main limiting factor for mass transfer and adsorption in the 3D printed monoliths. Protein adsorption and separation resolution can be greatly improved by 3D printing stationary phases with finer details, in line with the size of current adsorptive resins for chromatography of approximately 50 µm diameter. While typical DLP printers can produce pixel sizes down to 50 µm in the x-y plane, the printing of complex but continuous and connected features requires a minimum of 3 pixels width, corresponding to a minimum of 150 µm thickness. In addition, issues associated with light scattering from the UV light engine and digital mirror device apparatuses reduce the theoretical print resolution. Poor mechanical properties of models containing very fine struts further limit the minimum size that can be reliably 3D printed. Current developments are aiming to further decrease the printing resolution by employing higher resolution projectors, optimisation of the optics and light path to reduce scattering, and increase of the mechanical properties of the materials – also one of the goals of the current paper. As the 3D printing technology evolves, it is likely that the 3D printing of stationary phases with 50 µm feature size will be achieved in the near future. On the other hand, we are observing a shift in the biopharmaceutical market as it moves towards larger biological entities such as viral particles or

stem cells. These pose a major challenge to current downstream operations due to their structure complexity, shape, and size, with serious diffusional limitations even in traditional chromatographic stationary phases [24].

3.3.2. Purification of C-phycocyanin from solid-laden suspensions

Limitations in the resolutions of a 3D printer can be employed effectively as a positive attribute, with the fabrication of stationary phases with relatively large channels to allow the flow of cell- or particle- laden samples directly onto the column without the need for previous sample clarification [6]. This concept was proven here for the purification of CPC from unclarified *A. platensis* biomass. In particular, high-shear homogenised *A. platensis* biomass was fed directly to the 3D printed monoliths (Schoen gyroid, 50 % porosity, 500 µm walls, 3 mL CV) and the eluted fractions were assessed in relation to CPC purity and recovery.

The unclarified supernatant had to be tested in a custom-built set-up as it is not safe to employ the ÄKTA™ Pure system with solid-laden solutions. Accordingly, preliminary experiments were run with clarified feedstock (i.e. cell debris removed via centrifugation and filtration) on both the custom built and the ÄKTA™ Pure systems to compare the results across the two experimental platforms. These experiments also offer a benchmark to evaluate the separation performance of the novel 3D printed QA-materials. Good agreement was found for the purification of clarified CPC extracts across the two experimental systems (Figure 5-A), with average purification factors over the elution step of 2.8 and 3.1 for the custom-built and the ÄKTA™ Pure systems, respectively (Figure 5-C). Purities up to 4.0 were also recorded in the central fractions of the elution step, suggesting that different CPC fractions could be collected to suit different applications, e.g. pharmaceutical and/or analytical grade CPC. In particular, as also indicated by the A_{620} signal in Figure 5-A, the majority of CPC is eluted at the beginning of the elution step, with later fractions containing significantly less CPC and at the same time relatively higher amounts of co-eluting contaminants. This is also reflected in the trend of the purification factor presented in Figure 5-C, with an initial elution spike followed by a steady decline. An overall CPC recovery of 65 % and 54 % was measured with the custom-built and the

ÄKTA™ Pure systems, respectively. This is in line with the recovery measured in the batch adsorption experiments with BSA, confirming the need to optimize the conditions of the elution step to achieve complete recoveries. Most importantly, the consistency in the recovery data across experimental set-ups further validates the appropriateness of the custom-built rig to carry out chromatographic runs. The main apparent drawback of the custom-built apparatus lies in the higher noise of the measured results, ascribed to its manual handling and control, but with overall trends well matching the automated ÄKTA™ Pure system.

Direct application of crude CPC extracts resulted in a qualitatively similar chromatogram to the ones obtained feeding clarified CPC extracts (Figure 5-B). The flow-through during loading of the unclarified sample showed a significantly larger absorbance signal, consistent with the higher levels of proteinaceous contaminants present in the crude CPC extract. The recovered CPC in the pooled elution step showed an average purification factor of 2.7, in line with the runs with the clarified sample. This is further confirmed by the profile of the purification factor presented in Figure 5-C for all three cases studied here. The latter is a key result, as it demonstrates that the ligand-protein interactions and CPC adsorption were not affected by the presence of cell debris and other solid particulate in the feed. A recovery of 38 % was detected when using the crude CPC extract, somewhat lower than when using clarified CPC extracts. This is in line with complex binding behaviour of the multicomponent feed on the stationary phases [25].

Many procedures for the purification of CPC have been described in literature, most relying on a combination of multiple purification steps, usually including ammonium precipitation, dialysis, and packed bed AEX chromatography to achieve CPC purities of up to 6.7 [26–37]. The AEX chromatography step alone in packed bed mode provides purification factor ranging from 1.3 to 4.9. Reported single step CPC purification procedures from crude feedstocks are generally based on expanded bed adsorption (EBA) chromatography [32,33,38,39] or membrane chromatography [40]. Among these, EBA operates by fluidising the chromatographic particles thanks to an impinging upwards flow of the mobile phase, thus creating large pore space for the unhindered flow of the

solid-laden feed. This is conceptually similar to the 3D printed monolith here presented, with the flow-through channels designed prior to 3D printing in the three-dimensional CAD model. The proposed 3D printing approach embodies other advantages over EBA such as increased stability in the monolithic format over a fluidised bed generally hard to stabilise and operate, as well as the possibility to fine tune the channels to suit specific applications, e.g. suspensions containing different particulates, flow rates, viscosities, etc. [41]. Accordingly, the results obtained in this work are compared with past data reported for CPC purification using Q and DEAE Streamline media in EBA mode (Table 2). In particular, purification factors ranging between 2.7 and 4.8 were obtained with EBA, respectively, providing recoveries up to 79 % [32]. Moraes et al. [32] compared the purification of crude CPC extract using EBA (Streamline Q XL resin) to the purification of clarified extract (centrifugation and filtration) on packed bed Q-Sepharose FF, revealing a similar final purity of 1.6 and 1.7 and a purification factor of 3.2 and 2.8, respectively. This demonstrates that EBA provides the same purification power as a packed bed column, independent of the presence of cell debris in the applied sample. The same trend was demonstrated for DEAE functionalised chromatography beads, achieving a purification factor of 4.6 for a clarified CPC sample [42] and 4.8 for a crude CPC sample [33]. The purification factors for the 3D printed monoliths are in agreement with the reported values for commercial materials, and are independent of the initial sample purity (Table 2). Recovery in the elution step for the 3D printed monoliths is slightly lower than for commercial materials. While this is consistent with the adsorption results obtained with BSA, it further highlights the need to optimise the elution conditions, e.g. by appropriately modulating pH, ionic strength and/or flow rate of the elution buffer.

4. Concluding remarks

In this work we report a novel material formulation to produce QA monoliths in a single fabrication step through 3D printing technology, i.e. not requiring follow up activation and functionalization protocols to introduce ion exchange ligands. Optimization of the parent material composition

enabled overcome a number of hurdles associated with previous “one-step” 3D printable materials for chromatography, including improved protein binding through selection of appropriate ligand density, enhanced elution characteristics for higher protein recoveries, improved mechanical properties, more open porous microstructure to favour mass transfer within the stationary phase, and a more “customer-oriented” aesthetic appearance. The proposed material showed excellent protein binding capacity of up to 104 ± 10.6 mg/mL in batch adsorption experiments with BSA, comparable with commercially available QA materials [43].

After optimization, the QA material was tested in dynamic conditions for i) the separation of BSA and MYO as model proteins from a clear solution and ii) the purification of CPC from homogenized extracts containing cell debris, i.e. sample loaded with no clarification. This is the first demonstration to date that a 3D printed stationary phase can indeed enable protein separation and protein capture directly from solid-laden feeds. In particular, separation of BSA and MYO using a linear salt gradient demonstrated good reproducibility in terms of retention time and peak area for the two analysed proteins. The dimensions of the three dimensional gyroid were chosen to ensure reproducible and reliable printing process over chromatographic performance. This resulted in band broadening effects and poor resolution btw the two proteins due to mass transfer limitations into the 500 µm thick walls of the chromatographic material. We expect current limitations in the resolution of 3D printing technologies to be overcome in the near future, enabling fabrication of stationary phases with dimensions in the same order as preparative chromatography beads (50 µm). Resolution limitation was turned into an advantage by exploiting the large printed channels for the capture of CPC directly from cell-laden unclarified samples in a unit operation closely resembling expanded bed adsorption chromatography. The novel 3D printed QA-monolith enabled one-step capture and purification of CPC at food grade quality directly from a homogenised cell suspension. Also, purification factors observed were in line to performance observed on commercial materials for EBA chromatography. In contrast to EBA systems, notoriously difficult to control especially in term of maintaining a stable bed height [32], the 3D printed stationary phases are in monolithic format, with

Schoen gyroid structure reproducibly fabricated, ensuring excellent bed stability and consistency of results. In addition, the 3D printed monoliths enable removal of filtration and/or centrifugation steps for sample clarification, allowing a reduction in processing steps, processing times and costs. This is a key consideration, as product losses during downstream processing and purification are still the main cost in bioproduction.

We believe the results in this study set in stone the concept of directly 3D printed monoliths for chromatography. Future improvements in printing resolution together with bespoke stationary phase designs optimised for specific applications will enable a new paradigm in the chromatography arena.

jssc202000722-sup-0001-SuppMat.pdf

Supporting Information

Acknowledgements

We would like to thank IGM resin, BASF and Arkema for their continuous support and providing us with free samples. We also acknowledge the use of the Cryo FIB/SEM bought with the EPSRC grant EP/P030564/1 and Thomas Glen for help with the image acquisition. Ursula Simon would like to acknowledge the School of Engineering at the University of Edinburgh for funding her PhD scholarship. This project was co-funded by the Industrial Biotechnology Innovation Centre (IBioIC, grant number 2019-1-1) and ScotBio. Sarah Teworte would like to acknowledge the School of Engineering at the University of Edinburgh for funding her undergraduate summer research placement.

Conflict of interest statement: There are no conflicts of interest to declare.

REFERENCES

[1] Dolamore, F., Fee, C., Dimartino, S., Modelling ordered packed beds of spheres: The importance of bed orientation and the influence of tortuosity on dispersion. *J. Chromatogr. A*

2018, 1532, 150–160.

[2] Schure, M. R., Maier, R. S., Kroll, D. M., Davis, H. T., Simulation of ordered packed beds in chromatography. *J. Chromatogr. A* 2004, 1031, 79–86.

[3] Fee, C., 3D-printed porous bed structures. *Curr. Opin. Chem. Eng.* 2017, 18, 10–15.

[4] Fee, C., Nawada, S., Dimartino, S., 3D printed porous media columns with fine control of column packing morphology. *J. Chromatogr. A* 2014, 1333, 18–24.

[5] Macdonald, N. P., Currivan, S. A., Tedone, L., Paull, B., Direct Production of Microstructured Surfaces for Planar Chromatography Using 3D Printing. *Anal. Chem.* 2017, 89, 2457–2463.

[6] Fee, C. J., Dimartino, S., Huber, T., Separation Medium, WIPO Patent 2017103863A1, publ. date December 16, 2017.

[7] Simon, U., Dimartino, S., Direct 3D printing of monolithic ion exchange adsorbers. *J. Chromatogr. A* 2019, 1587, 119–128.

[8] Puzorjov, A., McCormick, A. J., Phycobiliproteins from extreme environments and their potential applications. *J. Exp. Bot.* 2020, 71, 3827–3842.

[9] Kuddus, M., Singh, P., Thomas, G., Al-Hazimi, A., Recent Developments in Production and Biotechnological Applications of C-Phycocyanin. *Biomed Res. Int.* 2013, 2013, 1–9.

[10] Gong, H., Beauchamp, M., Perry, S., Woolley, A. T., Nordin, G. P., Optical approach to resin formulation for 3D printed microfluidics. *RSC Adv.* 2015, 5, 3627–3637.

[11] Ligon, S. C., Liska, R., Stampfl, J., Gurr, M., Mülhaupt, R., Polymers for 3D Printing and Customized Additive Manufacturing. *Chem. Rev.* 2017, 117, 10212–10290.

[12] Wang, M.-M., Li, N., Ai, L.-F., Li, L., Chen, X.-L., Jia, Y.-Q., Wang, X.-S., Poly[(2-(acryloyloxy) ethyl]trimethylammonium chloride- co -ethylene dimethacrylate monolith on-line solid-phase

extraction coupled with liquid chromatography and tandem mass spectrometry for the fast determination of salicylic acid in foodstuffs. *J. Sep. Sci.* 2018, 41, 3432–3440.

[13] Mansour, F. R., Waheed, S., Paull, B., Maya, F., Porogens and porogen selection in the preparation of porous polymer monoliths. *J. Sep. Sci.* 2020, 43, 56–69.

[14] Courtois, J., Byström, E., Irgum, K., Novel monolithic materials using poly(ethylene glycol) as porogen for protein separation. *Polymer (Guildf).* 2006, 47, 2603–2611.

[15] Du, K.-F., Yang, D., Sun, Y., Fabrication of high-permeability and high-capacity monolith for protein chromatography. *J. Chromatogr. A* 2007, 1163, 212–218.

[16] Merhar, M., Podgornik, A., Barut, M., Žigon, M., Štrancar, A., Methacrylate monoliths prepared from various hydrophobic and hydrophilic monomers - Structural and chromatographic characteristics. *J. Sep. Sci.* 2003, 26, 322–330.

[17] Jungbauer, A., Chromatographic media for bioseparation. *J. Chromatogr. A* 2005, 1065, 3–12.

[18] Franke, A., Forrer, N., Butté, A., Cvijetić, B., Morbidelli, M., Jöhnck, M., Schulte, M., Role of the ligand density in cation exchange materials for the purification of proteins. *J. Chromatogr. A* 2010, 1217, 2216–2225.

[19] Wrzosek, K., Gramblička, M., Polakovič, M., Influence of ligand density on antibody binding capacity of cation-exchange adsorbents. *J. Chromatogr. A* 2009, 1216, 5039–5044.

[20] Li, Y., Lee, M. L., Biocompatible polymeric monoliths for protein and peptide separations. *J. Sep. Sci.* 2009, 32, 3369–3378.

[21] Jung, Y., Torquato, S., Fluid permeabilities of triply periodic minimal surfaces. *Phys. Rev. E* 2005, 72, 056319.

[22] Maskery, I., Sturm, L., Aremu, A. O., Panesar, A., Williams, C. B., Tuck, C. J., Wildman, R. D.,

Ashcroft, I. A., Hague, R. J. M., Insights into the mechanical properties of several triply periodic minimal surface lattice structures made by polymer additive manufacturing. *Polymer (Guildf).* 2018, 152, 62–71.

[23] Dolamore, F., In Silico Analysis of Flow and Dispersion in Ordered Porous Media, University of Canterbury, Christchurch, New Zealand, 2017.

[24] Moleirinho, M. G., Silva, R. J. S., Alves, P. M., Carrondo, M. J. T., Peixoto, C., Current challenges in biotherapeutic particles manufacturing. *Expert Opin. Biol. Ther.* 2020, 20, 451–465.

[25] Boi, C., Dimartino, S., Hofer, S., Horak, J., Williams, S., Sarti, G. C., Lindner, W., Influence of different spacer arms on Mimetic Ligand™ A2P and B14 membranes for human IgG purification. *J. Chromatogr. B* 2011, 879, 1633–1640.

[26] Silveira, S. T., De Menezes Quines, L. K., Burkert, C. A. V., Kalil, S. J., Separation of phycocyanin from Spirulina platensis using ion exchange chromatography. *Bioprocess Biosyst. Eng.* 2008, 31, 477–482.

[27] Liao, X., Zhang, B., Wang, X., Yan, H., Zhang, X., Purification of C-Phycocyanin from Spirulina platensis by Single-Step Ion-Exchange Chromatography. *Chromatographia* 2011, 73, 291–296.

[28] Patil, G., Chethana, S., Sridevi, A. S., Raghavarao, K. S. M. S., Method to obtain C-phycocyanin of high purity. *J. Chromatogr. A* 2006, 1127, 76–81.

[29] Kissoudi, M., Sarakatsianos, I., Samanidou, V., Isolation and purification of food-grade C-phycocyanin from Arthrospira platensis and its determination in confectionery by HPLC with diode array detection. *J. Sep. Sci.* 2018, 41, 975–981.

[30] Patel, A., Mishra, S., Pawar, R., Ghosh, P. K., Purification and characterization of C-Phycocyanin from cyanobacterial species of marine and freshwater habitat. *Protein Expr.*

Purif. 2005, 40, 248–255.

[31] Niu, J.-F., Wang, G.-C., Lin, X., Zhou, B.-C., Large-scale recovery of C-phycocyanin from Spirulina platensis using expanded bed adsorption chromatography. *J. Chromatogr. B* 2007, 850, 267–276.

[32] Moraes, C. C., Sala, L., Ores, J. da C., Braga, A. R. C., Costa, J. A. V., Kalil, S. J., Expanded and fixed bed ion exchange chromatography for the recovery of C-phycocyanin in a single step by using lysed cells. *Can. J. Chem. Eng.* 2015, 93, 111–115.

[33] Figueira, F. da S., Moraes, C. C., Kalil, S. J., C-Phycocyanin purification: Multiple processes for different applications. *Brazilian J. Chem. Eng.* 2018, 35, 1117–1128.

[34] Amarante, M. C. A. de, Corrêa Júnior, L. C. S., Sala, L., Kalil, S. J., Analytical grade C-phycocyanin obtained by a single-step purification process. *Process Biochem.* 2020, 90, 215–222.

[35] Boussiba, S., Richmond, A. E., Isolation and characterization of phycocyanins from the blue-green alga Spirulina platensis. *Arch. Microbiol.* 1979, 120, 155–159.

[36] Kumar, D., Dolly, Dhar, W., Pabbi, S., Kumar, N., Walia, S., Dhar, D. W., Pabbi, S., Kumar, N., Walia, S., Extraction and purification of C-phycocyanin from Spirulina platensis (CCC540). *Indian J. Plant Physiol.* 2014, 19, 184–188.

[37] Feng, Y., Li, X., Wen, Y., Bu, Y., Method for Preparing High Purity Phycobiliprotein with Primary Column Chromatography, China 200810134122, publ. date July 16, 2008.

[38] Moraes, C. C., da Costa Ores, J., Costa, J. A. V., Kalil, S. J., Recovery of C-Phycocyanin in the Presence of Cells Using Expanded Bed IEC. *Chromatographia* 2011, 74, 307–312.

[39] Chen, K.-H., Wang, S. S. S., Show, P.-L., Lin, G.-T., Chang, Y.-K., A rapid and efficient technique

for direct extraction of C-phycocyanin from highly turbid Spirulina platensis algae using hydrophobic interaction chromatography in stirred fluidized bed. *Biochem. Eng. J.* 2018, 140, 47–56.

[40] Lauceri, R., Chini Zittelli, G., Maserti, B., Torzillo, G., Purification of phycocyanin from Arthrospira platensis by hydrophobic interaction membrane chromatography. *Algal Res.* 2018, 35, 333–340.

[41] de Araújo, N. K., Pimentel, V. C., da Silva, N. M. P., de Araújo Padilha, C. E., de Macedo, G. R., dos Santos, E. S., Recovery and purification of chitosanase produced by Bacillus cereus using expanded bed adsorption and central composite design. *J. Sep. Sci.* 2016, 39, 709–716.

[42] Bermejo, R., Ramos, A., Pilot scale recovery of phycocyanin from spirulina platensis using expanded bed adsorption chromatography. *Chromatographia* 2012, 75, 195–204.

[43] Schmidt-Traub, H., Schulte, M., Seidel-Morgenstern, A., Preparative Chromatography. Third Edition, Wiley, Weinheim 2020.

Figure captions

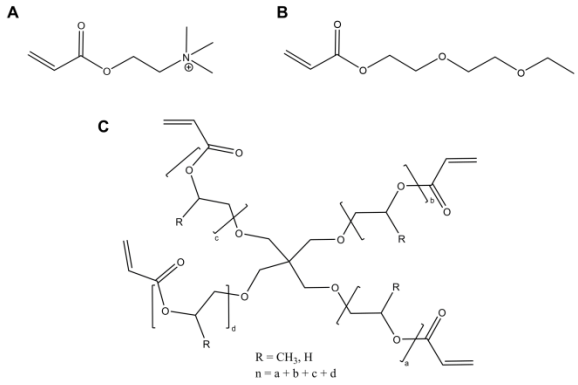

Figure 1: Chemical structures of the QA-functionalised monomer AETAC (A), non-functionalised monomer DEGEEA (B) and supercrosslinker SR494 (C) applied in this work.

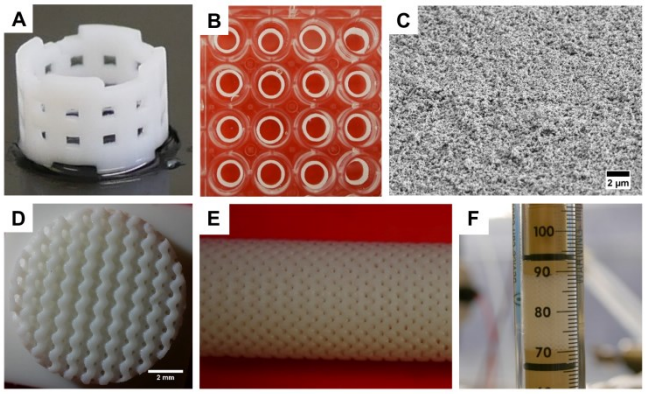

Figure 2: 3D printed QA-functionalised monoliths. (A) Hollow cylinder employed in batch adsorption (B) fitted into 96-well plate allowing in-situ measurement of protein concentration using a plate reader. (C) SEM image of 3D printed QA material with optimal ligand density of 1.73 mmol/mL. (D, E) Cylindrical Schoen gyroid structure (F) introduced in glass column for protein separation.

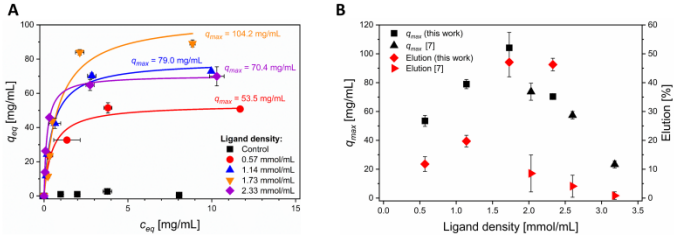

Figure 3: BSA adsorption onto the novel QA materials. (A) Equilibrium adsorption data together with best-fit Langmuir isotherm for different ligand densities (0, 0.57, 1.14, 1.73, 2.33 mmol/mL); (B) Maximum binding capacity, q_{max}, and percentage recovery during elution as a function of material's ligand density in comparison to the previously published material [7].

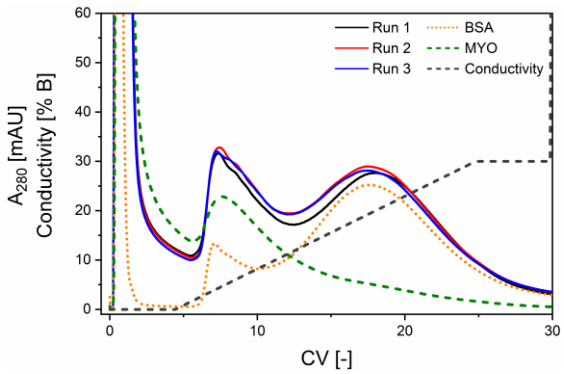

Figure 4: Separation of MYO and BSA using a 1.6 mL Schoen gyroid column with 50 % porosity and 500 µm walls. Three consecutive runs are shown providing reproducible retention times for MYO (7.0 ± 0.1 CV) and BSA (18.7 ± 0.1 CV). Large fraction (36.7 ± 1.3 %) of the injected protein was observed in flow through, indicating mass transfer issues from the large printed channels (500 µm) into the porous printing material.

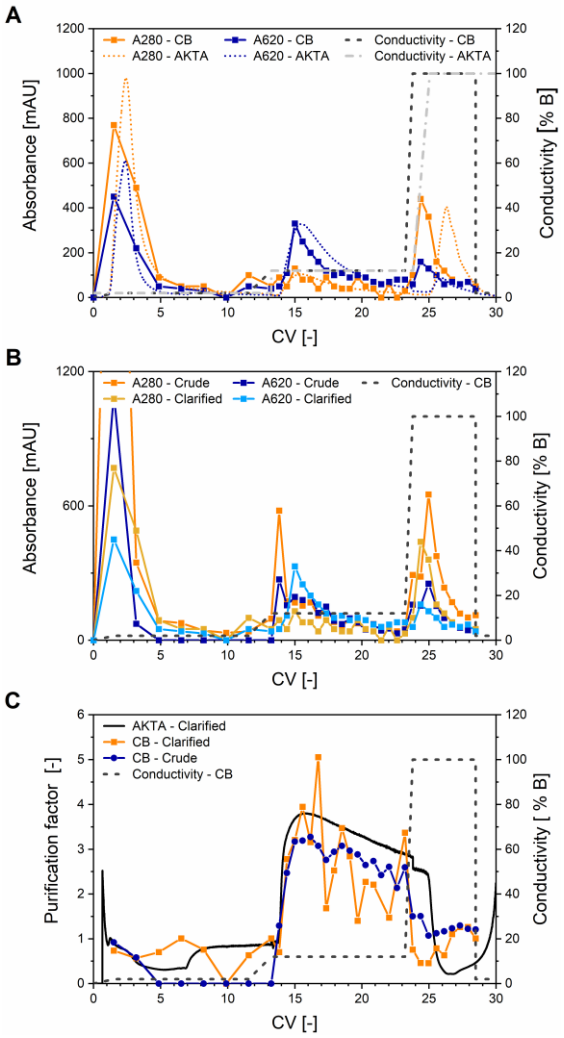

Figure 5: Chromatograms for CPC purification from *A. platensis* using 3D printed monolith with Schoen gyroid geometry (3 mL column volume, 50 % bed porosity, 500 µm wall thickness); A) Purification of clarified extract using an AKTA Pure in comparison to the custom-built (CB) liquid chromatography system; B) Comparison of CPC purification from clarified and crude CPC extracts on the custom-built system; C) Purification factor (A620/A280 normalised against initial sample's purity) for the three chromatographic runs.

TABLE 1 Langmuir best-fit parameters for the batch adsorption of BSA onto 3D printable materials with different ligand densities

	Ligand density [mmol/mL]			
	0.57	**1.14**	**1.73**	**2.33**
q_{max} **[mg/mL]**	53.5 ± 3.8	79.0 ± 3.2	104.2 ± 10.6	70.4 ± 2.0
k_D **[mg/mL]**	0.500 ± 0.151	0.513 ± 0.079	0.863 ± 0.270	0.181 ± 0.022
R^2	0.97	0.99	0.96	0.99

TABLE 2 Comparison of CPC purification performance of the novel 3D printed QA-monolith to commercial AEX resins in EBA mode

	Sample	Initial purity (A_{620}/A_{280}) [-]	Purification factor [-]	Recovery [%]	Reference
3D printed QA monolith	Clarified	0.79	2.8	65	This work
	Unclarified	0.36	2.7	38	This work
EBA: Streamline Q XL	Unclarified	0.5	3.2	79	[32]
		0.6	4.6	-	[38]
EBA: Streamline DEAE	Clarified	0.19	4.6	-	[42]
	Unclarified	0.6	2.7	59	[32]
		0.5	4.8	-	[33]